Performance Analysis of Time-Modulated Arrays for the Angle Diversity Reception of Digital Linear Modulated Signals

Roberto Maneiro-Catoira, *Student Member, IEEE,* Julio Brégains, *Senior Member, IEEE,* José A. García-Naya*, *Member, IEEE,* Luis Castedo, *Senior Member, IEEE*, Paolo Rocca, *Senior Member, IEEE* and L. Poli, *Member, IEEE,*

***Abstract*—Diversity occurs whenever several copies of the same transmitted signal arrive at a receiver. Such a situation allows for improving the performance of a wireless communication system transmitting over a radio channel without increasing the transmit power. Previous works have shown that time-modulated arrays are capable of faithfully acquiring digital signals while exploiting angular diversity through the adaptive beamforming of their harmonic patterns. In this work we take a step further and consider a wireless communication system employing digital linear modulated signals and an innovative receiver that includes a time-modulated array and a maximum ratio combining subsystem. The maximum ratio combiner is adapted to optimally exploit the multipath channel angular diversity. The performance of the system is analyzed in terms of two metrics: the signal-to-noise ratio and the symbol error rate. The results are compared to those achieved with other receivers that include conventional antenna arrays, exhibiting the time-modulated array solution a good trade-off between performance and hardware complexity.**

***Index Terms*—Antenna arrays, digital communication, time-modulated arrays, adaptive beamforming.**

I. Introduction

TIME-modulated arrays (TMAs) are antenna arrays whose radiated power pattern is controlled by periodically enabling and disabling the excitations of the individual array elements [1]. Such a periodic modulation is a nonlinear operation that generates sideband signals radiated at frequencies shifted from the carrier frequency at multiples of the time-modulation rate. Sideband radiation is usually considered a harmful phenomenon that may severely reduce the TMA gain because its power content may represent a significant portion of the total radiated power. The usual approach to consider the sideband radiation problem is to minimize its effect, which is not an easy task and requires sophisticated –usually multiobjective– optimization methods. Through such design methods, the TMA on/off sequences are determined to achieve a trade-off among sideband radiation, side-lobe levels, and efficiency [2]–[5], or even to handle the real-time adaptive nulling as an additional feature [6]. Complementary to software optimization, alternative hardware solutions were investigated to improve the efficiency of the switches [7] and to reduce the sideband radiation [8].

Nevertheless, sideband radiation is not necessarily a damaging phenomenon and can be profitably exploited to improve the performance of a TMA. In fact, the exploitation of the harmonic patterns enhances the TMA with smart-antenna capabilities, like beam-scanning [9], [10], adaptive beamforming [11]–[13], or beam steering and its applications as direction of arrival (DOA) estimation [14]–[18].

The use of TMAs for the transmission of communication signals still remains a challenge, although several encouraging research results are already available in the literature. For example, the signal frequency restrictions were already stated in [19], [20], and the transmission of analog signals was analyzed and experimentally evaluated in [21], [22]. An emerging and promising research topic is the influence of TMAs on the performance of wireless digital communications. In this sense, the feasibility of TMAs for linear digital modulations (LDM) was theoretically analyzed in [23], [24], while the signal-to-noise ratio (SNR) at the receiver for the simplest scenario (binary phase shift keying (BPSK) modulation and additive white gaussian noise (AWGN) channel) was considered in [25]. The multibeam characteristics of TMAs were also considered for space-division multiple access (SDMA) systems in [26], but the quantification of the performance was left as a future work. The performance of TMAs for digital communications in multipath scenarios was addressed in [27], considering systems that exploit multipath signals received over the TMA harmonic patterns. The results were compared to those based on conventional arrays with the same pattern shape as the one corresponding to the fundamental mode of the TMA, but without beamforming capacity. More recent works focus on the hardware design of TMAs applied to the spatial filtering of signals [28], and even for mm-Wave communications for interference suppression [29].

Up to the authors' knowledge, however, no previous study has addressed a performance comparison of TMAs with respect to other conventional beamforming adaptive arrays when applied to an LDM communication system over fading chan-

* Corresponding author: José A. García Naya, jagarcia@udc.es.

This work has been funded by Xunta de Galicia, MINECO of Spain, and FEDER funds of the EU under grants 2012/287 and TEC2013-47141-C4-1-R.

R. Maneiro-Catoira, J. Brégains, J.A. García-Naya, and L. Castedo are with the Department of Electronics and Systems at the University of A Coruña, 15071 A Coruña, Spain (email: roberto.maneiro@udc.es; julio.bregains@udc.es; jagarcia@udc.es; luis@udc.es).

P. Rocca and L. Poli are with the ELEDIA Research Center, University of Trento, Via Sommarive 5, I-38123 Trento, Italy (e-mail: paolo.rocca@unitn.it; lorenzo.poli@unitn.it).

Digital Object Identifier

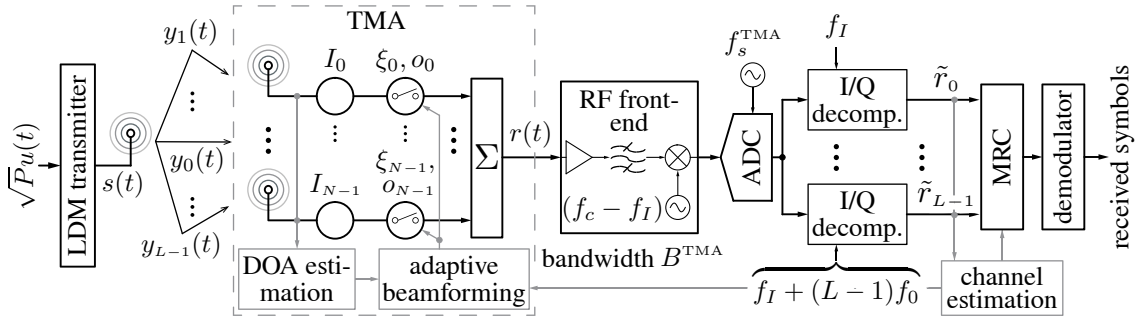

Fig. 1. Block diagram of a wireless system with an LDM transmitter equipped with an omni-directional antenna and a TMA for exploiting channel diversity at the receiver. A super-heterodyne transceiver architecture is assumed for the receiver, although a direct-conversion design is also possible. The signal at the TMA output $r(t)$ (with a bandwidth B^{TMA}) is first down-converted to f_I and digitized by the ADC (with a sampling frequency f_s^{TMA}). Next, for each of the L branches, the signals are I/Q decomposed (the I/Q digital decomposition frequency corresponding to the i-th branch is $f_I + mf_0$), filtered, and decimated. Finally, the obtained discrete-time $\tilde{r}_i$ symbols are forwarded to the MRC, producing an improved version of the received symbol $\tilde{r}$ which is finally sent to the digital demodulator to estimate the transmitted symbol from the received one.

nels. In this sense, the contribution of this work is three-fold. 1) The introduction of key aspects for signal transmission (e.g. SNR per path or antenna efficiency) in the synthesis of harmonic beamforming with TMAs. 2) The derivation of closed-form expressions for the SNR per path, the average SNR, and the symbol error rate (SER) at reception, as functions of the TMA parameters, allowing for synthesizing ad-hoc TMAs for multipath narrowband communication purposes. And 3), the comparison of TMAs both in terms of performance and complexity with respect to other conventional beamforming adaptive arrays when applied to an LDM communication system over a realistic fading channel.

LDMs are widely used because of their high spectral efficiency, especially when the number of modulation levels is large [30, Chapter 5, p. 140]. In addition, LDMs are often combined with powerful error correction codes to become power efficient. On the other hand, TMAs can be used to perform adaptive beamforming, exploiting the multipath channel diversity without the need of phase shifters [31].

In this work we consider a narrowband wireless communication system using an M-ary LDM as shown in Fig. 1. We assume an omni-directional antenna at the transmitter and a TMA at the receiver. The signal propagates over different paths (with distinct lengths) and arrives at the receiver from multiple directions. Therefore, the receiver observes multiple replicas of the transmitted signal with different amplitudes and time-delays. In such a scenario, a TMA allows for obtaining an equivalent single input multiple output (SIMO) system that exploits the angle diversity of the channel by means of adaptive beamforming. Under certain assumptions, this receiver faithfully recovers L multipath replicas of the transmitted signal, making a profitable use of them. Although we will see in detail those assumptions in the forthcoming analysis, we next present an overview of the whole system.

We consider a multipath wireless channel. The different path gains are modeled as zero-mean complex-valued statistically-independent Gaussian-distributed random variables. Such a channel is referred to as Rayleigh fading channel (RFC) and is an adequate model for non-line-of-sight (NLOS) scenarios [32, Chapter 2, p. 18]. According to this model, each wireless fading path introduces a random change on the amplitude and on the delay of the transmitted signals. Given that we are considering narrowband communications, such time-delays are assumed to be small enough compared to the symbol duration in order to avoid inter-symbol interference (ISI). We assume that at the receiver we have knowledge of the DOA of the L signal replicas to make feasible the TMA adaptive beamforming capabilities (see Fig. 1). More specifically, the beamforming is done with the first $L-1$ positive harmonic patterns of the TMA (excluding the fundamental mode), i.e., those at frequencies $f_c \pm mf_0, m = 1, \ldots, L-1$, f_0 is the TMA pulse frequency, and f_c the carrier frequency. We also assume that the signal replica $y_0(t)$ has a DOA that coincides with the maximum of the TMA fundamental mode pattern and hence there is no need for beamforming with the fundamental mode. The beamforming will satisfy the spatial orthogonality among all the TMA radiation patterns (fundamental and harmonics) in the directions of their respective maximums to avoid interference between the replicas [31]. On the other hand, we assume perfect channel state information (CSI) [32, Chapter 7, p. 159] at the receiver when determining the MRC parameters. Regarding the frequencies involved in the data transmission process, the TMA pulse frequency (f_0) and the signal bandwidth (B) must satisfy the condition $f_0 > 2B$ to avoid overlapping [23]. We also assume, for the sake of simplicity, that there are no interference signals impinging on the TMA at $f_c + mf_0$. Finally, the noise at the receiver is modeled as AWGN [33, Chapter 1, p. 33].

The remainder of the paper is structured as follows. Section II presents the considered TMA, its radiation characteristics, and the equivalent baseband model for each multipath component. Such a model is used in Section III to quantify the average SNR per symbol at each MRC input branch. Next, Section IV characterizes the SER of such a system when M-ary LDM signals are transmitted, thus allowing for comparing the performance of the system with respect to other approaches based on conventional arrays. Section V analyzes the trade-off between the TMA efficiency and the number of multipath components to be exploited. The systems included for comparison purposes are described in Section VI. More

specifically, the receiver shown in Fig. 1 is compared 1) to a single input single output (SISO) system (which does not exploit channel diversity) using a conventional array that has a radiation pattern with the same spatial shape as that of the TMA fundamental mode, but provided with a higher gain because it is not affected by sideband radiation; and 2) to a SIMO system equipped with a conventional array and an adaptive linear beamforming network (LBFN) capable of synthesizing simultaneously a set of spatial radiation patterns with the same shapes as those generated by the TMA in its operating frequencies (fundamental and harmonics) but, in this case, at a single frequency f_c. Section VII presents the results from numerical simulations. Finally, Section VIII is devoted to the conclusions.

II. Characterization of the Diversity Paths

Let us consider that the receive antenna in Fig. 1 is a linear TMA with N isotropic elements distributed along the z axis. Let $g_n(t)$ be the periodic pulse train (with fundamental period T_0 and fundamental frequency $f_0 = 1/T_0$) that controls the n-th array element. Pulses are often rectangular since in this case they can be easily implemented with switches. Since $g_n(t)$ is a periodic signal, it can be represented by its Fourier series expansion. The q-th coefficient of such a series is given by [11]

$$G_{nq} = \xi_n \operatorname{sinc}(q\pi\xi_n)\mathrm{e}^{-jq\pi(\xi_n+2o_n)}, \tag{1}$$

where $\operatorname{sinc}(x) = \sin(x)/x$ denotes the sinc function, $n \in \Upsilon = \{0, \ldots, N-1\}$, $\xi_n \in (0,1) \subset \mathbb{R}$ are the normalized pulse time durations and $o_n \in [0, 1-\xi_n] \subset \mathbb{R}$ the switch-on instants, respectively. On the other hand, the array factor with the term $\mathrm{e}^{j2\pi(f_c+qf_0)t}$ explicitly included, $F_q^{\text{TMA}}(\theta,t)$, corresponding to the harmonic frequency $q\omega_0$ is given by [22]

$$F_q^{\text{TMA}}(\theta,t) = \mathrm{e}^{j2\pi(f_c+qf_0)t}\sum_{n=0}^{N-1} G_{nq} I_n \mathrm{e}^{jkz_n\cos\theta}, \tag{2}$$

where z_n represents the n-th array element position on the z-axis, $I_n = |I_n|\mathrm{e}^{j\varphi_n}$ is the complex static current excitation in polar form ($|I_n|$ is its modulus and φ_n is its phase), θ is the angle with respect to the array main axis, k is the wavenumber, and f_c is the carrier frequency.

The optimization of the periodic pulse trains $g_n(t)$ often focuses on the generation of suitable harmonic beams. Notice that when only the fundamental beam ($q = 0$) is exploited, the TMA will acquire the desired signal over the pattern $F_0^{\text{TMA}}(\theta,t)$. However, TMAs are able to simultaneously receive multiple replicas arriving from different directions over the higher order harmonic patterns $F_q^{\text{TMA}}(\theta,t)$ with $q \neq 0$.

Figure 1 shows a block diagram of a wireless digital communication system capable of exploiting channel diversity. At the receiver, the signals $y_m(t)$ (with $m \in \Psi = \{0,1,\ldots,L-1\}$), each one corresponding to the m-th multipath signal component, are acquired through a TMA that performs beamforming with the first $L-1$ harmonic patterns. At the output of the TMA, each multipath signal component appears at its own carrier frequency $f_c + mf_0$ (with $m \in \Psi$). Assuming $f_0 > 2B$, being B the signal bandwidth, implies that there is no overlapping in the frequency domain between the multipath signals and they can be down-converted to an intermediate frequency f_I by a conventional RF front-end with the only requirement of supporting the additional bandwidth required by the $L-1$ signal multipath components. After the down-converter, multipath signal components appear at frequencies $f_I + mf_0$.

In the next step, the signals are converted to the digital domain by means of a single ADC configured with a sampling frequency f_s^{TMA} high enough, given the bandwidth B^{TMA} occupied by all multipath signal components. At each demodulator branch, the digital signal is first I/Q decomposed (i.e., the passband signal at the ADC output is converted to its equivalent baseband representation), and finally, the demodulation (including the decimation) takes place. As a result, $\tilde{r}_m[n]$ symbols (with $m \in \Psi$) corresponding to the L multipath signal components are obtained.

Next, the signals are forwarded to the MRC, which optimally combines the L multipath replicas and produces an improved version of the received signals to be forwarded to the LDM demodulator. Notice that the main objective of the MRC is to maximize the SNR of the received symbol [32, Chapter 9, p. 262]. Note also that the approach typically followed by multiple-antenna receivers based on MRC requires a complete receiver chain (antenna, RF front-end, and ADC) for each of the L branches, while the TMA approach allows for using a single receiver chain although requiring a larger bandwidth.

A. Baseband Model for the Diversity Paths

In this subsection we derive the baseband-equivalent model for each of the L multipath signal components in Fig. 1. We assume an LDM transmit signal

$$s(t) = \sqrt{P}u(t)\mathrm{e}^{j2\pi f_c t}, \tag{3}$$

where P represents the transmit power, and $u(t)$ is the equivalent baseband representation of $s(t)$ [23]. The transmit signal $s(t)$ propagates over an L-path wireless channel, arriving at the TMA along the directions θ_m, with $m \in \Psi$. Let $y_m(t)$ be the signal impinging on the TMA over the multipath angle θ_m after being attenuated and time-delayed, i.e.,

$$y_m(t) = \alpha_m s(t-\tau_m) = \alpha_m\sqrt{P}u(t-\tau_m)\mathrm{e}^{j2\pi f_c(t-\tau_m)}, \tag{4}$$

where α_m and τ_m are the attenuation factor and time-delay of the m-th multipath, respectively.

With respect to the wireless channel, the TMA, and the receiver, we assume the following:

- the directions θ_m, the attenuations α_m, and the delays τ_m are statistically independent random variables for each path m, with $m \in \Psi$, and known to the system designer to ensure a fair performance comparison between the considered systems regardless channel estimation errors;
- given that we are considering narrow-band communications, the time-delays satisfy $\tau_m \ll 1/B$. Hence, $u(t-\tau_m) \approx u(t)$ and (4) can be rewritten as

$$y_m(t) = \alpha_i\sqrt{P}u(t)\mathrm{e}^{j2\pi f_c t}\mathrm{e}^{-j2\pi f_c\tau_m} = \alpha_m\mathrm{e}^{-j\phi_m}s(t), \tag{5}$$

with $\phi_m = 2\pi f_c\tau_m$ being the phase shift introduced by τ_m;

- the m-th path channel response $h_m = \alpha_m \mathrm{e}^{-j\phi_m}$ is modeled as a complex normal (CN) zero-mean circularly-symmetric random variable. This model is particularly valid when considering a multipath clustered environment, in which case the channel response is the result of the sum of all the multipath responses within a cluster. Hence, by virtue of the central limit theorem, it is reasonable to model h_m as a CN zero-mean circularly-symmetric random variable [34, Chapter 2, p. 36]. Consequently, α_m is Rayleigh-distributed with a mean square value
$$\Omega_m = \mathrm{E}[|h_m|^2], \tag{6}$$
where $E[x]$ stands for the expectation of x, and ϕ_m is uniformly distributed in $[0, 2\pi)$. This channel model is known in the literature as RFC [32, Chapter 2, p. 18];
- it is possible to synthesize the TMA radiation patterns such that $F_m^{\mathrm{TMA}}(\theta_m, t)$, with $m \in \Psi$, is maximized along the m-th path direction θ_m, while the remaining paths are filtered-out, i.e., $F_m^{\mathrm{TMA}}(\theta_l, t) \approx 0\ \forall m \neq l$ with $m, l \in \Psi$ [31]. As a consequence, the $r_m(t)$ signals at the output of the TMA are orthogonal in frequency;
- the signal replica $y_0(t)$ impinges on the TMA through the direction corresponding to the maximum of the TMA fundamental mode pattern;
- $|F_q^{\mathrm{TMA}}(\theta_m, t)|^2 \ll |F_l^{\mathrm{TMA}}(\theta_m, t)|^2$, for $m, l \in \Psi$ and $q \geq L$, i.e., only the first L patterns of the TMA are considered while the rest are minimized;
- in order to avoid spectral signal overlapping, the bandwidth B of $u(t)$ and the TMA frequency f_0 fulfill $f_0 > 2B$ and $f_c \gg f_0$ [23]; and finally,
- the spectrum occupied by all multipath signal components at the output of the TMA is free of interferences from other signals, i.e., the carriers $f_c + mf_0$, with $m \in \Psi$ are occupied only with the received signals $y_m(t)$.

At the TMA output, the received signal $r_m(t)$ over the $F_m(\theta, t)$ radiation pattern is the superposition of all multipath signals plus the AWGN noise $\nu_m(t)$,
$$r_m(t) = \sum_{l=0}^{L-1} F_m^{\mathrm{TMA}}(\theta_l, t) y_l(t) + \nu_m(t). \tag{7}$$
Recall that the radiation pattern satisfies $F_m(\theta_l, t) \approx 0$, $\forall m \neq l$, and that the signal received over the TMA m-th pattern appears at the frequency $f_c + mf_0$. Hence (7) simplifies to
$$r_m(t) = \alpha_m \mathrm{e}^{-j\phi_m} F_m^{\mathrm{TMA}}(\theta_m, t)\sqrt{P}u(t)\mathrm{e}^{j2\pi(f_c+mf_0)t} + \nu_m(t), \tag{8}$$
where $y_l(t)$ was substituted by its definition in (5) for a carrier frequency $f_c + mf_0$.

A TMA exhibits a nonlinear behavior due to the application of periodic (with fundamental frequency f_0) rectangular pulses to the array excitations. Taking (2) into account, the array factor of the TMA is
$$\begin{aligned} F^{\mathrm{TMA}}(\theta, t) &= \sum_{q=-\infty}^{\infty} F_q^{\mathrm{TMA}}(\theta, t) \\ &= \sum_{q=-\infty}^{\infty} \mathrm{e}^{j2\pi(f_c+qf_0)t} \sum_{n=0}^{N-1} G_{nq} I_n \mathrm{e}^{jkz_n \cos\theta}, \end{aligned} \tag{9}$$

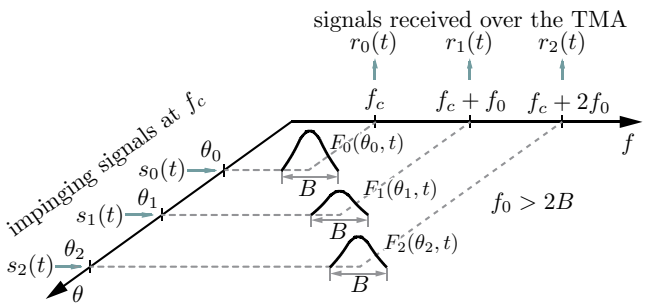

Fig. 2. Behavior of the TMA. The signals received over the TMA harmonic patterns are translated into the corresponding harmonic frequencies.

where G_{nq} are the Fourier coefficients of the periodic rectangular pulses (see (1)), which depend on the pulse durations ξ_n and on the switch-on instants o_n. By properly choosing G_{nq} (that is, ξ_n and o_n), and under the conditions defined above in this section, it is possible to *window* the useful harmonics as much as possible. Then, (9) can be rewritten as
$$F^{\mathrm{TMA}}(\theta, t) \approx \sum_{q=-(L-1)}^{L-1} \mathrm{e}^{j2\pi(f_c+qf_0)t} \sum_{n=0}^{N-1} G_{nq} I_n \mathrm{e}^{jkz_n \cos\theta} \tag{10}$$
to obtain orthogonal patterns that, jointly with the condition $f_0 > 2B$, allow for taking advantage of the aforementioned nonlinear behavior as shown in Fig. 2. Therefore, narrowband multipath signals whose carrier frequency is f_c can be received over the different TMA harmonic patterns, which are translated into the corresponding harmonic frequencies.

The received signal $r(t)$ at the TMA output is the superposition of all received signals $r_m(t)$ and occupies a total bandwidth $B^{\mathrm{TMA}} = (L-1)f_0 + B/2$, with B being the bandwidth of $s(t)$. Therefore, the sampling frequency of the ADC must satisfy the Nyquist criterion, i.e.,
$$f_s^{\mathrm{TMA}} > 2(f_I + (L-1)f_0 + B/2), \tag{11}$$
where f_I is the intermediate carrier frequency at the output of the down-converter.

On the other hand, the baseband equivalent of the m-th received signal $r_m(t)$ at each TMA element output can be written as
$$\tilde{r}_m(t) = \alpha_m \mathrm{e}^{-j\phi_m} F_m^{\mathrm{TMA}}(\theta_m, t)\sqrt{P}u(t) + \tilde{\nu}_m(t), \tag{12}$$
with $\tilde{\nu}_m(t)$ the baseband equivalent AWGN in $\tilde{r}_m(t)$ as the superposition of all individual noise contributions.

In summary, the operations carried out by the TMA followed by the RF front-end and the L I/Q digital demodulators shown in Fig. 1 can be interpreted as a SIMO subsystem that produces L multipath replicas from the signal transmitted. The baseband equivalent representation of such a SIMO subsystem is shown in Fig. 3.

III. Average SNR per Symbol and Path

In a context where a wireless digital communication system is subject to fading impairments, the average SNR is an adequate metric of the overall system performance since it

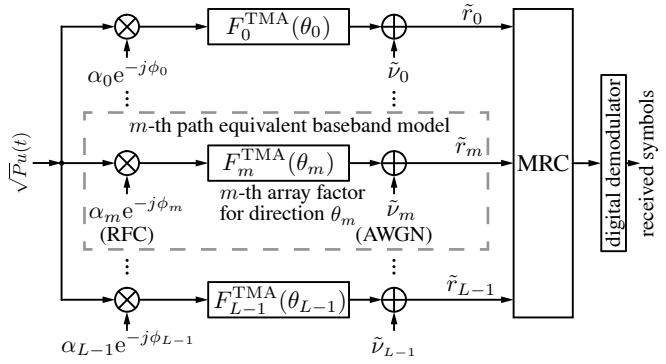

Fig. 3. Equivalent baseband representation of the TMA-based wireless digital communication system shown in Fig. 1 that exploits the L multipath replicas from the transmitted signal $s(t)$ through an RFC.

quantifies the received signal fidelity. Given that the instantaneous SNR per symbol at the m-th branch in Fig. 3 is a random variable and is given by

$$\gamma_m^{\text{TMA}} = \alpha_m^2 G_m^{\text{TMA}} E_s/N_0, \tag{13}$$

where E_s is the average energy per transmitted symbol, N_0 is the AWGN power spectral density, α_m^2 is the instantaneous power of the m-th multipath channel component, G_m^{TMA} is the antenna gain accounting for the power received in the direction of the peak radiation with respect to an isotropic source and is given by [35]

$$G_m^{\text{TMA}} = \eta_{\text{TMA}} \frac{4\pi |F_m^{\text{TMA}}(\theta_m, t)|^2}{P_R^{\text{TMA}}}. \tag{14}$$

Let us study in detail the different variables in (14). A crucial parameter in this analysis is the total efficiency of the TMA given by

$$\eta_{\text{TMA}} = \eta_s \cdot \eta(L), \tag{15}$$

η_s being the efficiency of the network switch [7] that accounts for the absorption of energy when the switches are off, and $\eta(L)$ being the TMA power efficiency when $L-1$ harmonics[1] are exploited in addition to the fundamental mode. Such power efficiency is defined as the ratio between the useful mean received power P_U^{TMA} and the total mean received power P_R^{TMA}, i.e.,

$$\eta(L) = \frac{P_U^{\text{TMA}}}{P_R^{\text{TMA}}} = \frac{\sum_{q=0}^{L-1} p_q}{\sum_{q=-\infty}^{\infty} p_q}, \tag{16}$$

[1]As $g_n(t)$ is a real signal, its Fourier coefficients verify $G_{nq} = G^*_{n(-q)}$, and it is easy to prove (see (2)) that $|F_q^{\text{TMA}}(\theta, t)|^2 = |F_{-q}^{\text{TMA}}(\pi - \theta, t)|^2$, unavoidably synthesizing a couple of diagrams for q and $-q$, which are symmetric with respect to $\theta = \pi/2$. This lack of independence between couples of harmonic patterns of the same order does not match with the randomness nature of the DOAs. Therefore, we restrict the adaptive beamforming either to the positive or the negative harmonics to achieve an adequate level of flexibility. This fact limits the power efficiency of the system shown in Fig. 1. The feasibility of independence between harmonic patterns of the same order in a TMA needs to be overcome in future works.

where p_q is the total mean received power at the q-th harmonic when a carrier is received over a TMA, and is given by [23]

$$p_q = 4\pi \left[\sum_{n=0}^{N-1} |I_n|^2 |G_{nq}|^2 + 2 \sum_{n=0}^{N-1} \sum_{\substack{l=0 \\ l\neq n}}^{N-1} \text{Re}\{I_l I_n^* G_{lq} G_{nq}^*\} \,\text{sinc}(k(z_l - z_n)) \right]. \tag{17}$$

On the other hand, by considering (1) and (2), we can easily quantify $|F_m^{\text{TMA}}(\theta_m, t)|^2$ as

$$|F_m^{\text{TMA}}(\theta_m, t)|^2 = \sum_{n=0}^{N-1} \xi_n^2 \,\text{sinc}^2(m\pi\xi_n) + 2 \sum_{n=0}^{N-1} \sum_{\substack{l=0 \\ l\neq n}}^{N-1} |I_l||I_n| \xi_l \xi_n \,\text{sinc}(m\pi\xi_l) \,\text{sinc}(m\pi\xi_l) \cdot \cos\{m\pi[\Delta\xi_{nl} + 2\Delta o_{nl}] + k\Delta z_{nl} \cos\theta_m - \Delta\varphi_{nl}\}, \tag{18}$$

with $\Delta\xi_{nl} = \xi_n - \xi_l$, $\Delta o_{nl} = o_n - o_l$, $\Delta z_{nl} = z_n - z_l$, and $\Delta\varphi_{nl} = \varphi_n - \varphi_l$.

Once analyzed in detail the different components of G_m^{TMA}, we can obtain, by virtue of (13), the average SNR per symbol[2] at the m-th branch in Fig. 3, arriving at

$$\overline{\gamma}_m^{\text{TMA}} = \text{E}[\alpha_m^2 G_m^{\text{TMA}} E_s/N_0] = \Omega_m G_m^{\text{TMA}} E_s/N_0, \tag{19}$$

where Ω_m is the mean square value of α_m^2 (recall (6)).

Therefore, by substituting, on the one hand, (17) into (16) and (16) into (15) and, on the other, (15) and (18) into (14), and finally, (14) into (19), we obtain a closed-form expression (in (44) such an expression is shown for a particular case) for the average SNR $\overline{\gamma}_m^{\text{TMA}}$ in terms of the TMA parameters (ξ_n, o_n), the number of paths exploited (L), the average power of the fading path (Ω_m), and the ratio of the average energy per transmitted symbol to the AWGN power spectral density (E_s/N_0). Finally, the average SNR at the output of the MRC is the sum of the individual average SNR values at the L input branches, i.e.,

$$\overline{\gamma}^{\text{TMA}}(\xi_n, o_n, L, \Omega_m, E_s/N_0) = \sum_{m=0}^{L-1} \overline{\gamma}_m^{\text{TMA}}, \tag{20}$$

with $\overline{\gamma}_m^{\text{TMA}}$ defined in (19), in contrast to the average SNR at the input of the MRC, which is L times smaller than $\overline{\gamma}^{\text{TMA}}$.

IV. Average SER Characterization

The average SER is another widely used figure of merit for the evaluation of digital communication systems (DCSs). The average SER for a digital receiver with an instantaneous input SNR γ is determined as

$$\text{SER} = \int_0^{\infty} P_S(e|\gamma) p(\gamma) d\gamma, \tag{21}$$

[2]Note that $\overline{\gamma}_m = \text{E}[\gamma_m] = \int_0^{\infty} \gamma_m p(\gamma_m) d\gamma_m$ is the average SNR per symbol, where $p(\gamma_m)$ denotes the probability density function (PDF) of γ_m which, for the case of RFC, is $p(\gamma_m) = \frac{\gamma_m}{\overline{\gamma}_m} e^{-\frac{\gamma_m}{\overline{\gamma}_m}}, \gamma_m \geq 0$ [33].

with $P_{\mathrm{S}}(e|\gamma)$ the conditional SER for a given instantaneous SNR γ, and $p(\gamma)$ the PDF of γ. Recall that there exist closed-form expressions, in terms of the Gaussian Q-function, for the conditional SER of the majority of the most widely used LDM formats [30, Chapter 5, p. 140]. The average SER is obtained after solving the integral in (21).

According to Fig. 1, the input signal to the demodulator is the output signal from the MRC. The instantaneous SNR at the MRC output relates to the instantaneous SNR values at the MRC input branches as $\gamma = \sum_{m=0}^{L-1} \gamma_m$. Hence, in order to determine the average SER we must average the L dimensional conditional SER values $P_{\mathrm{S}}(e|\gamma_0, \gamma_1, \ldots, \gamma_{L-1})$ over the joint PDF $p(\gamma_0, \gamma_1, \ldots, \gamma_{L-1})$ of the instantaneous SNR values $\gamma_0, \gamma_1, \ldots \gamma_{L-1}$. Since the random variables γ_m are assumed to be statistically independent, $p(\gamma_0, \gamma_1, \ldots, \gamma_{L-1}) = \prod_{m=0}^{L-1} p(\gamma_m)$, and the averaging procedure results in

$$\mathrm{SER} = \underbrace{\int_0^{\infty} \cdots \int_0^{\infty}}_{L-\text{fold}} P_{\mathrm{S}}(e|\gamma_o \ldots \gamma_{L-1}) \prod_{m=0}^{L-1} p(\gamma_m) d\gamma_0 \ldots \gamma_{L-1}. \tag{22}$$

For the case of LDM signals, $P_{\mathrm{S}}(e|\gamma_0, \gamma_1, \ldots, \gamma_{L-1})$ is a Gaussian Q-function of the form [32, Chapter 9, p. 267]

$$P_{\mathrm{S}}(e|\gamma_0, \gamma_1, \ldots, \gamma_{L-1}) = Q\left(\sqrt{2 g_{\mathrm{MOD}} \sum_{m=0}^{L-1} \gamma_m}\right), \tag{23}$$

where g_{MOD} is a parameter depending on the LDM format and the constellation size M. For the most widely used LDM the value of such a parameter is

$$g_{\mathrm{ASK}} = 3/(M^2 - 1) \tag{24}$$

$$g_{\mathrm{PSK}} = \sin^2(\pi/M) \tag{25}$$

$$g_{\mathrm{QAM}} = 3/(2(M - 1)), \tag{26}$$

Solving the integral (22) is difficult. However, by considering an alternative expression of $Q(\cdot)$, the conditional SER (23) can be expressed as [36]

$$P_{\mathrm{S}}(e|\gamma_0, \gamma_1, \ldots, \gamma_{L-1}) = \frac{1}{\pi} \int_0^{\frac{\pi}{2}} \mathrm{e}^{-\frac{g_{\mathrm{MOD}} \sum_{m=0}^{L-1} \gamma_m}{\sin^2 \varrho}} d\varrho. \tag{27}$$

Substituting (27) into (22) and having in mind that for the RFC model $p(\gamma_m)$ is an exponential PDF with mean $\overline{\gamma}_m$, the following expressions for the average SER corresponding to ASK, PSK and QAM modulation formats [37] are obtained:

$$\mathrm{SER}_{\mathrm{ASK}} = \tfrac{2(M-1)}{M\pi} \int_0^{\frac{\pi}{2}} \prod_{m=0}^{L-1} \left(1 + \frac{\overline{\gamma}_m g_{\mathrm{ASK}}}{\sin^2 \varrho}\right)^{-1} d\varrho, \tag{28}$$

$$\mathrm{SER}_{\mathrm{PSK}} = \frac{1}{\pi} \int_0^{\frac{(M-1)\pi}{M}} \prod_{m=0}^{L-1} \left(1 + \frac{\overline{\gamma}_m g_{\mathrm{PSK}}}{\sin^2 \varrho}\right)^{-1} d\varrho, \tag{29}$$

$$\mathrm{SER}_{\mathrm{QAM}} = \frac{4}{\pi}\left(1 - \tfrac{1}{\sqrt{M}}\right) \left\{ \int_0^{\frac{\pi}{2}} \prod_{m=0}^{L-1} \left(1 + \frac{\overline{\gamma}_m g_{\mathrm{QAM}}}{\sin^2 \varrho}\right)^{-1} d\varrho - \right.$$

$$\left. - \left(1 - \tfrac{1}{\sqrt{M}}\right) \int_0^{\frac{\pi}{4}} \prod_{m=0}^{L-1} \left(1 + \frac{\overline{\gamma}_m g_{\mathrm{QAM}}}{\sin^2 \varrho}\right)^{-1} d\varrho \right\}, \tag{30}$$

Recall also that when considering the receiver with TMA shown in Fig. 1, the average SNR $\overline{\gamma}_m$ is $\overline{\gamma}_m^{\mathrm{TMA}}$ given by (19).

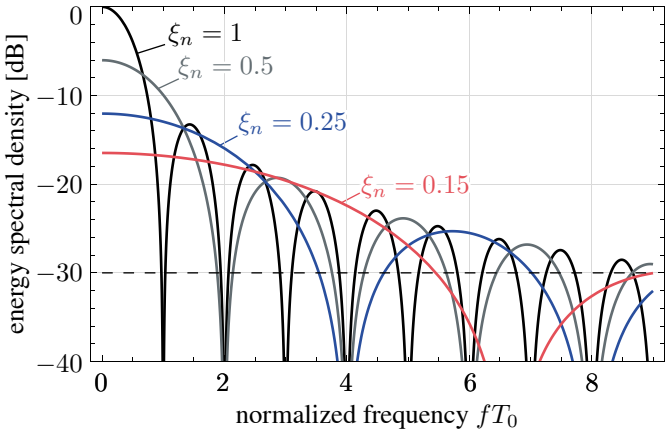

Fig. 4. Frequency-normalized ESD of a rectangular pulse, $|G_n(f)|^2$, for different values of ξ_n. The squared amplitude of the n-th excitation corresponding to the m-th harmonic pattern can be graphically identified in the plot as $|I_{nm}^{\mathrm{TMA}}|^2 = G_{nm}^2 = |G_n(m)|^2$.

Hence, under the assumptions established in Section II-A, we can plot the average SER in terms of the SNR per symbol E_s/N_0 with a closed-form expression involving the TMA synthesis parameters.

V. Trade-off Between the TMA Efficiency and L

In view of (1) and (2), and assuming $|I_n| = 1$, the squared modulus of the dynamic excitations of the m-th harmonic pattern are given by

$$\left|I_{nm}^{\mathrm{TMA}}\right|^2 = G_{nm}^2 = \xi_n^2 \,\mathrm{sinc}^2(\pi m \xi_n), \qquad n \in \Upsilon. \tag{31}$$

On the other hand, and according to the Fourier series expansion theory, G_{nm}^2 are a set of N samples –at the fixed harmonic frequency $f = m/T_0$– taken from each $|G_n(f)|^2$, with $G_n(f)$ the Fourier transform of the basic rectangular pulse (with a width ξ_n) that constitutes the periodic train $g_n(t)$. By normalizing the frequency axis with respect to $f_0 = 1/T_0$ we have that

$$\left|I_{nm}^{\mathrm{TMA}}\right|^2 = |G_n(m)|^2, \qquad n \in \Upsilon, \tag{32}$$

and therefore, to include successive harmonics ($fT_0 = 1, 2, 3, \ldots$) below the main lobe of the energy spectral density (ESD) of each pulse, it is necessary to reduce ξ_n properly (see Fig. 4). However, note that ξ_n cannot be too close to zero because, in such a case, the efficiency of the TMA, $\eta_{\mathrm{TMA}} = \eta_s \cdot \eta(L)$, will be significantly degraded, and consequently, the average SNR per path $\overline{\gamma}_m^{\mathrm{TMA}}$ will also be reduced.

Hence, for a given L –determined by the number of harmonics to be exploited in the beamforming– it is necessary to synthesize a TMA, according to the efficiency requirements, with the largest possible ξ_n values, hence enabling the corresponding $\mathrm{sinc}(\cdot)$ functions in Fig. 4 to incorporate such harmonics. At the same time, the values of ξ_n, together with o_n, must be able to shape the corresponding radiation patterns.

VI. Linear Beamforming

In order to better understand the impact on the performance of a digital communication system when considering a TMA

at reception, in this section we will analyze the performance of such a system when an array with linear beamforming is considered.

A. Linear Beamforming without Angular Diversity

We start considering a conventional array with a linear beamformer (LB) capable of synthesizing the same radiation pattern as that of the fundamental beam of a TMA (see Fig. 5). Recall that this radiation pattern points the maximum towards the main multipath direction θ_0 while it cancels the remaining ones. Hence, the receiver in this case cannot exploit the angular diversity of the multipath channel. The baseband equivalent representation of the receiver shown in Fig. 3 reduces to a SISO system.

The radiation pattern of the fundamental mode of the TMA in Fig. 1 can be accomplished with an LB by choosing the array complex excitations as the elements of the column vector $\mathbf{w}_0$ given by $w_{n+1}^0 = G_{n0} I_n \mathrm{e}^{-jkz_n \cos\theta_0} = I_n \xi_n \mathrm{e}^{-jkz_n \cos\theta_0}$, $n \in \Upsilon$. The array now provides a single signal whose baseband equivalent representation is

$$\tilde{r}_0(t) = \alpha_0 \mathrm{e}^{-j\phi_0} F^{\mathrm{LB}}(\theta_0, t)\sqrt{P} u(t) + \tilde{\nu}_0(t). \tag{33}$$

Recall that the equivalent channel response now depends on $F^{\mathrm{LB}}(\theta_0, t)$, namely the array factor of the LB towards the main multipath direction θ_0.

We next determine the average SNR per symbol at the output of the LB. The expression is similar to (19):

$$\overline{\gamma}^{\mathrm{LB}} = \mathrm{E}[\alpha_0^2 G^{\mathrm{LB}} \tfrac{E_s}{N_0}] = \Omega_0 G^{\mathrm{LB}} E_s/N_0, \tag{34}$$

with

$$G^{\mathrm{LB}} = 4\pi |F^{\mathrm{LB}}(\theta_0, t)|^2 / P_{\mathrm{R}_0}^{\mathrm{LB}} > G_0^{\mathrm{TMA}}. \tag{35}$$

Note that the parameter $\eta(L)$, inherent to the sideband radiation phenomenon, is not present in an LB. Recall that $|F^{\mathrm{LB}}(\theta, t)|^2 = |F_0^{\mathrm{TMA}}(\theta, t)|^2$ and hence it can be computed from (18). Finally, the power received by the LB, $P_{\mathrm{R}}^{\mathrm{LB}}$, can be calculated as the total mean received power over the array factor $F^{\mathrm{LB}}(\theta, t)$, i.e.,

$$P_{\mathrm{R}}^{\mathrm{LB}} = \int_0^{2\pi} \int_0^{\pi} |F^{\mathrm{LB}}(\theta, t)|^2 \sin(\theta) d\theta d\varphi. \tag{36}$$

On the other hand, remember that the average SER can be obtained for each LDM format by particularizing Eqs. (28) to (30) for $L = 1$ and $\overline{\gamma}_0 = \overline{\gamma}^{\mathrm{LB}}$ as in (34).

B. Linear Beamforming with Angular Diversity

It is possible to consider an LBFN to exploit the angular diversity in a multipath radio channel. The idea is to design an LB to receive each of the L multipath signals. Then, the signals provided by the LBs are linearly combined with an MRC to obtain a signal with improved SNR. Fig. 6 plots the block diagram of a DCS receiver with an LBFN and an MRC.

We assume that the LBFN is able to synthesize L spatial radiation patterns with the same shapes as the ones generated by the TMA at its different harmonic frequencies. Since the beamforming network is linear, all the radiation patterns perform at the same frequency f_c. As mentioned above, such radiation patterns point to a different multipath direction while they cancel the other ones. In this manner the LBFN provides different replicas of the transmitted signal and allows the receiver to exploit the channel angular diversity. The baseband equivalent representation of the receiver now corresponds to the SIMO system shown in Fig. 6.

TABLE I
COMPLEXITY COMPARISON BETWEEN THE PROPOSED TMA SYSTEM (SEE FIG. 1) AND THE TWO ALTERNATIVES CONSIDERED: LB AND LBFN (SEE FIGS. 5 AND 6, RESPECTIVELY).

	RF front-ends	**ADCs**	**demodulators**	**MRC**
TMA	1^*	$1^{\#}$	L	yes
LB	1	1	1	no
LBFN	L	L	L	yes

*: requires a larger bandwidth ($B^{\mathrm{TMA}} > B$).
$^{\#}$: requires a higher sampling frequency ($f_s^{\mathrm{TMA}} > f_s$).

The LBFN weights for the m-th beam are $w_{n+1}^m = G_{nm} I_n \mathrm{e}^{-jkz_n \cos\theta_m}$, with $m \in \Psi$ and $n \in \Upsilon$ as in (1). Such elements are collected into the column vector $\mathbf{w}_m$. The phase adjustment in each w_n^m is physically carried out by phase shifters having an insertion loss at f_c represented by $K_{\mathrm{ps}} < 1$ (and expressed in natural units). In this case, the generic m-th path model is similar to that developed in Section II, but modifying the gain terms. Instead of $F_m^{\mathrm{TMA}}(\theta_m, t)$ we now have $K_{\mathrm{ps}} F_m^{\mathrm{LB}}(\theta_m)/L$ due to the existence of the phase shifters and the L-way power splitters necessary to implement the LBFN. Under these circumstances, the average SNR for the m-th path is given by (19):

$$\overline{\gamma_m}^{\mathrm{LBFN}} = \mathrm{E}\left[\alpha_m^2 \frac{K_{\mathrm{ps}} G_m^{\mathrm{LBFN}}}{L} \frac{E_s}{N_0}\right] = \Omega_m \frac{K_{\mathrm{ps}} G_m^{\mathrm{LBFN}}}{L} \frac{E_s}{N_0}, \tag{37}$$

with

$$G_m^{\mathrm{LBFN}} = 4\pi |F_m^{\mathrm{LBFN}}(\theta_m, t)|^2 / P_{\mathrm{R}_m}^{\mathrm{LBFN}} > G_m^{\mathrm{TMA}}, \tag{38}$$

Again, $|F_m^{\mathrm{LBFN}}(\theta_m, t)|^2 = |F_m^{\mathrm{TMA}}(\theta_m, t)|^2$ and thus $|F_m^{\mathrm{LBFN}}(\theta_m, t)|^2$ can be obtained from (18). Correspondingly, $P_{\mathrm{R}_m}^{\mathrm{LBFN}}$ is calculated by plugging $F(\theta, t) = F_m^{\mathrm{LBFN}}(\theta_m, t)$ in (36). Similarly to (20), the average SNR at the MRC output is

$$\overline{\gamma}^{\mathrm{LBFN}} = \sum_{m=0}^{L-1} \overline{\gamma_m}^{\mathrm{LBFN}}, \tag{39}$$

Finally, the average SER for the different M-ary LDM formats can be determined for a given E_s/N_0 by plugging $\overline{\gamma_m} = \overline{\gamma_m}^{\mathrm{LBFN}}$ –as in (37)– into Eqs. (28) to (30).

C. Hardware Complexity Comparison

Table I shows the resources required by each of the three considered systems: TMA, LB, and LBFN[3]. Remarkably, the

[3] Notice that the sampling frequency corresponding to the ADCs in the LBFN shown in Fig. 5 must satisfy (11). Therefore, the minimum sampling frequencies of both systems satisfy $f_s^{\mathrm{TMA}} - f_s^{\mathrm{LBFN}} = 4(L-1)B$, whereas the percentage increase in the sampling frequency when the TMA is used with respect to the LBFN is given by $\Delta f_s[\%] = \left((f_s^{\mathrm{TMA}} - f_s^{\mathrm{LBFN}})/f_s^{\mathrm{LBFN}}\right) \cdot 100 = 4(L-1)/(2(f_I/B)+1) \cdot 100$, and we observe that if $f_I \gg B$, then $\Delta f_s[\%]$ is very low (recall that L is upper bounded due to the trade-off with the TMA efficiency), and therefore, it is even possible to use the same ADC for both solutions.

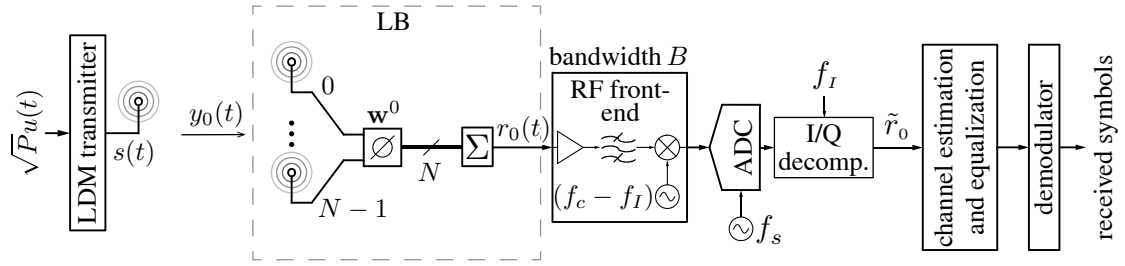

Fig. 5. Block diagram of the system in Fig. 1 but using a receiver equipped with a single linear beamformer (LB) having a radiation pattern with the same spatial shape as the TMA fundamental one. This receiver only acquires a single replica $y_0(t)$ of the transmitted signal and cannot exploit channel diversity.

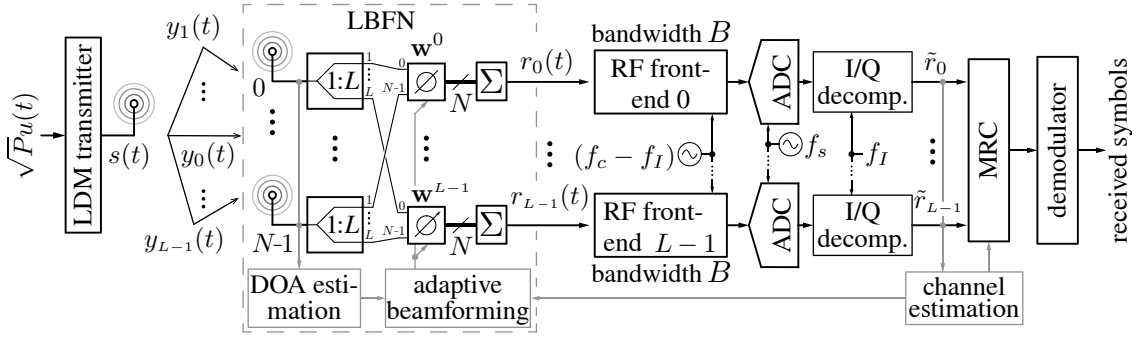

Fig. 6. Block diagram of the system in Fig. 1 but now using a receiver equipped with an LBFN consisting of a conventional array (excitation weights $\mathbf{w}^0$) plus a set of adaptive LBs ($\mathbf{w}^m$, $m = 1, \ldots, L-1$). Such an LBFN simultaneously synthesizes a series of spatial radiation patterns with the same shapes as those generated by the TMA. There are N elements, each one connected to an L-way power splitter, while the power splitters are connected to L phase shifters (the first one is static).

TMA solution is cheaper, in terms of hardware complexity, than the LBFN approach. Nevertheless, as described in Section II-A, in the TMA-based approach the ADC sampling frequency and the RF front-end bandwidth grow linearly with the number of multipath components L. On the other hand, the MRC is needed in both TMA and LBFN, but the latter is considerably more complex in terms of hardware, requiring additional power splitters and phase shifters. Obviously, the LB solution, as it does not exploit the diversity of the channel, is the simplest and cheapest one.

VII. Performance Comparison

A. TMA Assumptions: Simplified Expressions

Under the assumptions of uniform amplitude for the static currents, as well as an inter-element distance of half a wavelength, i.e.,

$$|I_n| = 1, \forall n \in \Upsilon, \text{ and } d = \Delta z_{nl} = \lambda/2, \tag{40}$$

the calculation of P_R^{TMA} in the denominator of (16) reduces to

$$P_R^{\text{TMA}} = 4\pi \sum_{n=0}^{N-1} \sum_{q=-\infty}^{\infty} |G_{nq}|^2 = 4\pi \sum_{n=0}^{N-1} \xi_n^2 \sum_{q=-\infty}^{\infty} \text{sinc}^2(q\pi\xi_n). \tag{41}$$

Having now in mind that for all $\xi_n \in (0,1)$ the sinc-square infinite series converges to

$$\sum_{q=-\infty}^{\infty} \text{sinc}^2(q\pi\xi_n) = 1/\xi_n, \tag{42}$$

we arrive at a simplified version of (41)

$$P_R^{\text{TMA}} = 4\pi \sum_{n=0}^{N-1} \xi_n. \tag{43}$$

Finally, by considering the assumptions (40) in (18), and substituting (18) together with (43) into (14), and finally (14) into (19), we arrive at the following closed-form expression

$$\begin{aligned}\overline{\gamma}_m^{\text{TMA}} = {} & \frac{\eta_s \Omega_m \sum_{q=0}^{L-1} \sum_{n=0}^{N-1} \xi_n^2 \,\text{sinc}^2(q\pi\xi_n)}{\left(\sum_{n=0}^{N-1} \xi_n\right)^2} \cdot \frac{E_s}{N_0} \cdot \\ & \cdot \Bigg[\sum_{n=0}^{N-1} \xi_n^2 \,\text{sinc}^2(m\pi\xi_n) + \\ & + 2 \sum_{n=0}^{N-1} \sum_{\substack{l=0 \\ l \neq n}}^{N-1} \xi_l \xi_n \,\text{sinc}(m\pi\xi_l) \,\text{sinc}(m\pi\xi_l) \cdot \\ & \cdot \cos\{m\pi[\Delta\xi_{nl} + 2\Delta o_{nl}] + \pi\cos\theta_m - \Delta\varphi_{nl}\} \Bigg], \end{aligned} \tag{44}$$

which gives the average SNR per symbol at the m-th MRC input branch in terms of the network parameters.

B. Description of the TMA Synthesis Method

The method is based on the same optimization algorithm proposed in [31, Section III.A], the particle swarm optimization (PSO), but some innovations have been introduced, both in the TMA architecture and at the algorithm level in order to optimize the metrics established in (28)-(30) when the TMA

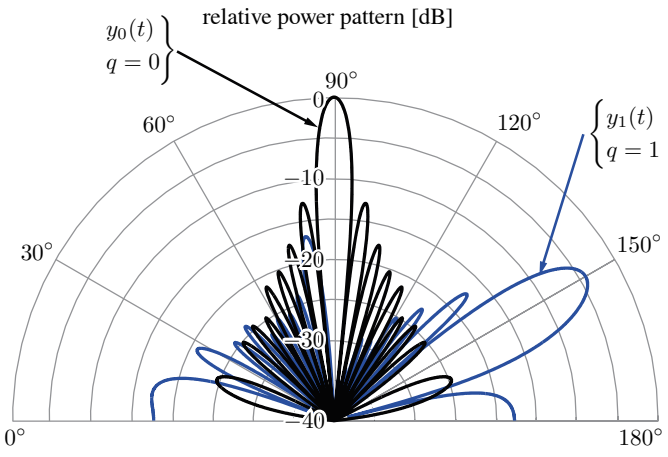

Fig. 7. Optimized radiation receiving pattern implementing the simplest configuration for the system in Fig. 1. Only the first harmonic ($L = 2$) of the TMA is exploited for adaptive beamforming. Notice the high level of mutual spatial orthogonality of the diagrams in the respective DOAs ($\theta_0 = 90°$ and $\theta_1 = 150°$).

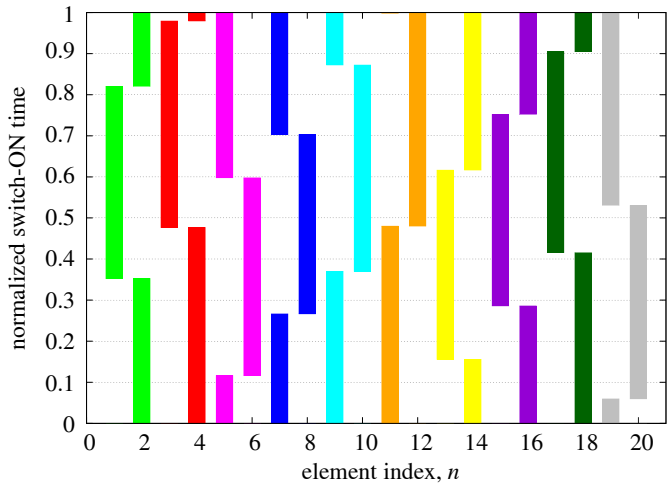

Fig. 8. Plot of the normalized time sequences which synthesize the radiation receiving pattern in Fig. 7.

beamforming is applied to digital communications in multipath scenarios. Such improvements on the technique of [31] are:

- The use of multi-throw switches, (i.e. the use of a single RF switch for the control of two adjacent elements) in order to simultaneously maximize both factors of the TMA efficiency, namely η_s, and $\eta(L)$. The PSO has been properly customized to only generate pairs of complementary pulses, as requested for the control of this new employed type of switches. As compared to the previous solutions, the new obtained results have demonstrated improved or even ideal η_s [7]. In the subsequent examples, single-pole triple-throw (SP3T) switches are used to exploit up to a L=3 multipath channel. For each switch, two throws are connected to a consecutive pair of elements of the array. For the case of $L = 2$ the third throw will not be programmed or used, and for the case $L = 3$ such a throw is used as the off state.
- The weighting coefficients used in the fitness function

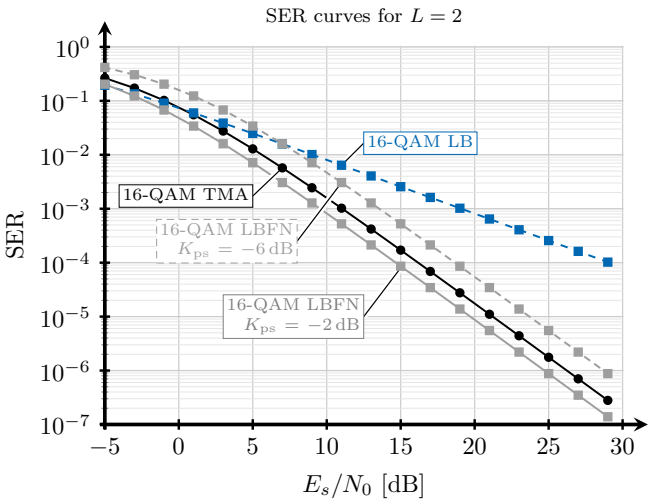

Fig. 9. SER curves comparing the performance of the SIMO TMA system with other solutions based on conventional arrays for the case of $L = 2$ (a two-path channel).

(see [31, Eq. 10]) have been adapted to the particular features of a signal-performance oriented scenario, aimed to safeguard the TMA efficiency and the SNR at the receiver. In this sense, the relative weight of the orthogonalization functional has been increased while the other weights on the side-lobe levels (SLL) functional as well as on the "equalization among the patterns maximums" functional, relatively relaxed.

C. Multipath Channel with $L = 2$

The simplest scenario capable of exploiting the TMA angle diversity according to Fig. 1 involves only the first harmonic pattern to carry out the adaptive beamforming. For the numerical simulations we take into account the following considerations:

- The average gain of the channel paths are identical and normalized, i.e., $\Omega_0 = \Omega_1 = 1$;
- The LDM considered is the quadrature amplitude modulation (QAM) with $M = 16$. The operational frequencies are: $f_c = 2.4\,\text{GHz}$, $f_0 = 500\,\text{kHz}$, $f_I = 10\,\text{MHz}$ and $B = 150\,\text{kHz}$. These numbers lead to ADC sampling frequencies satisfying $f_s^{\text{TMA}} > 21.15\,\text{MHz}$ and $f_s > 20.15\,\text{MHz}$; Fig. 7 shows the TMA optimized receiving radiation pattern considered for the analysis, which is synthesized with the normalized time sequences given in Fig. 8 whose ON and OFF instants for the TMA pulses are complementary. It is also remarkable the good level of orthogonalization between the patterns. Both characteristics, complementarity and orthogonality, are dictated by the algorithm described in Section VII-B.
- The resulting switches network efficiency is $\eta_s = 1$

(0 dB)[4] (as the switches never acquire the OFF state) and as the TMA power efficiency calculated through (16) is found to be $\eta(L) = 0.7$ (-1.55 dB), and according to (15) we arrive at an $\eta_{\text{TMA}} = 0.7$ (-1.55 dB);

- The LBFN described in Section VI-B includes phase shifters. As the insertion loss K_{ps} of a phase shifter strongly depends on the carrier frequency (varying from -2 to -13 dB), and we arbitrarily choose the S-band, we have considered two scenarios for the LBFN: an optimistic one with $K_{\text{ps}} = -2$ dB, and a pessimistic with $K_{\text{ps}} = -6$ dB according to the typical values at the f_c considered (see, for example, [38]);
- Finally, a set of SER[5] curves with respect to the E_s/N_0 is considered for the 16-QAM case. The SER curves are obtained by plugging the corresponding values for $\overline{\gamma}_m$ into (30).

Fig. 9 shows the aforementioned SER curves with respect to the E_s/N_0. From Fig. 9 it can be concluded that in this particular case the proposed TMA solution exhibits a significant performance improvement with respect to the LB-based approach and presents a competitive behavior with respect to the LBFN-based solution. This is because the TMA-based system can extract all the diversity ($L = 2$) offered by the channel, as the LBFN-based system does, while the LB-based solution only acquires a single replica of the received signal, thus not exploiting any channel diversity. This effect is clearly shown by the slope of the SER curves in Fig. 9: the higher the slope, the more diversity is extracted from the channel.

D. Multipath Channel with $L = 3$

We have also considered a scenario (see Fig. 10) with three impinging signals, where:

- The considerations about the gain of the channel paths, the LDM, the frequencies and the insertion losses K_{ps} in the LBFN are the same as those given in Section VII-C.
- The radiation pattern shown in Fig. 10 is synthesized with the pulse sequences given in Fig. 11. Note that due to the trade-off between L and the η_{TMA} –analyzed in Section V– it is not possible a perfect complementarity between a sequence and the following, i.e. it is necessary to have an OFF interval.
- Now $\eta_s = 0.62$ (-2.08 dB) (because the switches are OFF a fraction of the time) and since the TMA power efficiency is $\eta(L) = 0.61$ (-2.15 dB), we arrive at an $\eta_{\text{TMA}} = 0.38$ (-4.23 dB);

[4]For any of the described TMA efficiencies (switches network, power or total efficiencies) —generally symbolized here as η– the corresponding values of $10\log_{10}(\eta)$ in decibels are also provided in brackets in the text, after the corresponding value in natural units. Such values expressed in decibels can be considered as losses inherent to the TMA technique, and are useful for an easier comparison with other techniques such as LBFN.

[5]For a given scenario of DOAs, improved efficiency at the expense of a worse "equalization among patterns maximums" is a trade-off present in the TMA design. Therefore, different radiation patterns (with a distinct set of $|F_m^{\text{TMA}}(\theta_m, t)|^2$ but also associated to a distinct η_{TMA}) may lead to the same behavior in terms of SER. Quantitatively, sets of different values of $|F_m^{\text{TMA}}(\theta_m, t)|^2$ and η_{TMA} in Eqs. (14) and (19) may conduct to identical SER values in Eqs. (28) to (30). Under these circumstances, the designer decides the best solution from a radiation pattern point of view.

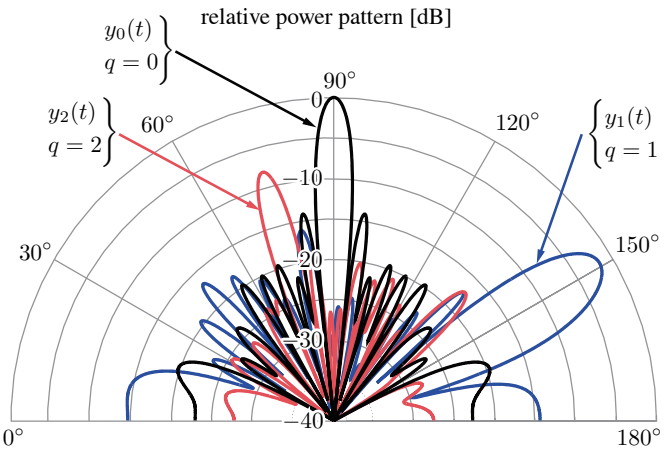

Fig. 10. Optimized radiation receiving pattern implementing the configuration for the system in Fig. 1 exploiting two harmonics ($L = 3$) of the TMA for adaptive beamforming. Notice the level of mutual spatial orthogonality between the diagrams in the respective DOAs ($\theta_0 = 90°$, $\theta_1 = 150°$, and $\theta_2 = 74°$).

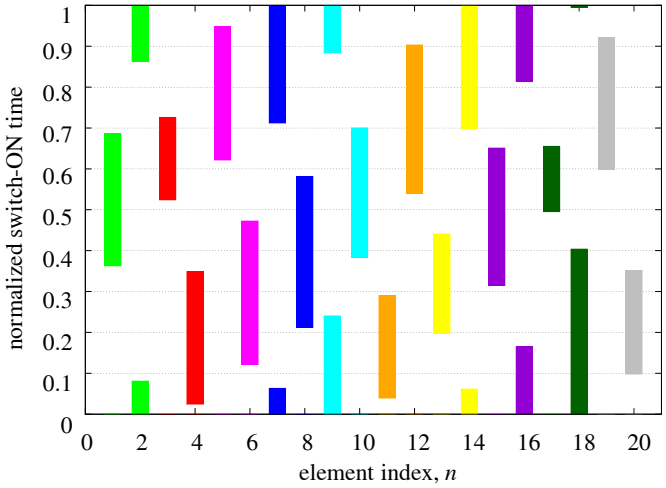

Fig. 11. Plot of the normalized time sequences which synthesize the radiation receiving pattern in Fig. 10.

- The curves in Fig. 12 show the behavior of the TMA compared to those of both the LBFN and the LB. In spite of the efficiency penalization due to the smaller ξ_n, the TMA is comparable to the LBFN for its more pessimistic scenario. Recall that for $L = 3$, the benefits of the TMA with respect to the LBFN in terms of the system hardware complexity are really remarkable (see Table I). Note also that if the carrier frequency were arbitrarily higher –for example 6 GHz– the behavior of both systems would converge because typical values of K_{ps} increase with the carrier frequency [38].

VIII. Conclusions

We proposed a wireless communication receiver consisting of a TMA performing nonlinear beamforming followed by an MRC subsystem devoted to extract channel diversity in form of angular diversity captured by the sideband radiation exhibited by the TMA. We considered the transmission of

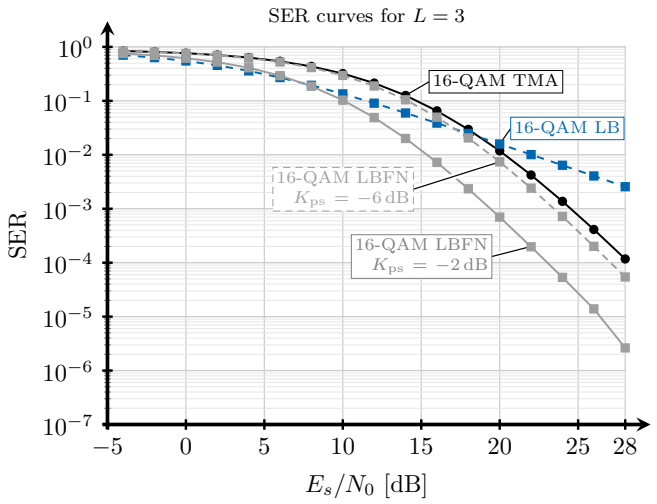

Fig. 12. SER curves comparing the performance of the SIMO TMA system with other solutions based on conventional arrays for the case of $L = 3$ (a three-path channel).

LDM signals through an RFC exhibiting channel diversity. As a reference, we compared the performance of the TMA-based receiver to that exhibited by a single LB-based receiver (thus not exploiting channel diversity) and to that offered by an LBFN-based receiver (also equipped with an MRC). We derived closed-form expressions for the SER with respect to the SNR when LDM signals are transmitted and considering the three aforementioned receivers. Remarkably, the SER of the TMA-based receiver can be expressed directly in terms of the main parameters of the TMA itself, hence providing a fundamental tool for the designer. A new optimization algorithm to synthesize the radiation pattern conditioned to a specific architecture that allows for maximizing the TMA efficiency was implemented.

Finally, numerical simulations for the cases of two and three incoming signal replicas were also presented. The SER versus SNR results showed that both TMA-based and LBFN-based receivers were able to profitably exploit the channel diversity. Such SER versus SNR results also illustrated that the TMA exhibits the best trade-off between hardware and software complexity with respect to the performance obtained. Due to the compromise between L and the TMA power efficiency, inherent to the rectangular pulses, there is still room for improving the beamforming performance with TMAs by exploring more appropriate shapes for the basic pulses $g_n(t)$, as well as in the preprocessing of such pulses to achieve full independence between different harmonic patterns.

REFERENCES

[1] W. Kummer, A. Villeneuve, T. Fong, and F. Terrio, "Ultra-low sidelobes from time-modulated arrays," *IEEE Transactions on Antennas and Propagation*, vol. 11, no. 6, pp. 633–639, 1963.

[2] L. Poli, P. Rocca, L. Manica, and A. Massa, "Handling sideband radiations in time-modulated arrays through particle swarm optimization," *IEEE Transactions on Antennas and Propagation*, vol. 58, no. 4, pp. 1408–1411, April 2010.

[3] S. K. Mandal, G. K. Mahanti, and R. Ghatak, "Differential evolution algorithm for optimizing the conflicting parameters in time-modulated linear array antennas," *Progress In Electromagnetics Research B*, vol. 51, pp. 101–118, 2013.

[4] S. Pal, S. Das, and A. Basak, "Design of time-modulated linear arrays with a multi-objective optimization approach," *Progress In Electromagnetics Research B*, vol. 23, pp. 83–107, 2010.

[5] L. Poli, P. Rocca, L. Manica, and A. Massa, "Pattern synthesis in time-modulated linear arrays through pulse shifting," *IET Microwaves, Antennas Propagation*, vol. 4, no. 9, pp. 1157–1164, September 2010.

[6] P. Rocca, L. Poli, G. Oliveri, and A. Massa, "Adaptive nulling in time-varying scenarios through time-modulated linear arrays," *IEEE Antennas and Wireless Propagation Letters*, vol. 11, pp. 101–104, 2012.

[7] Q. Zhu, S. Yang, R. Yao, and Z. Nie, "Gain improvement in time-modulated linear arrays using SPDT switches," *IEEE Antennas and Wireless Propagation Letters*, vol. 11, pp. 994–997, 2012.

[8] Y. Tong and A. Tennant, "Reduced sideband levels in time-modulated arrays using half-power sub-arraying techniques," *IEEE Transactions on Antennas and Propagation*, vol. 59, no. 1, pp. 301–303, Jan 2011.

[9] H. Shanks, "A new technique for electronic scanning," *IRE Transactions on Antennas and Propagation*, vol. 9, no. 2, pp. 162–166, March 1961.

[10] G. Bogdan, Y. Yashchyshyn, and M. Jarzynka, "Time-modulated antenna array with lossless switching network," *IEEE Antennas and Wireless Propagation Letters*, vol. PP, no. 99, pp. 1–1, 2016.

[11] L. Poli, P. Rocca, G. Oliveri, and A. Massa, "Harmonic beamforming in time-modulated linear arrays," *IEEE Transactions on Antennas and Propagation*, vol. 59, no. 7, pp. 2538–2545, July 2011.

[12] G. Li, S. Yang, Y. Chen, and Z. Nie, "A hybrid analog-digital adaptive beamforming in time-modulated linear arrays," *Electromagnetics*, vol. 30, no. 4, pp. 356–364, 2010.

[13] Y. Tong and A. Tennant, "A two-channel time modulated linear array with adaptive beamforming," *IEEE Transactions on Antennas and Propagation*, vol. 60, no. 1, pp. 141–147, Jan 2012.

[14] G. Li, S. Yang, Y. Chen, and Z.-P. Nie, "A novel electronic beam steering technique in time modulated antenna array," *Progress In Electromagnetics Research*, vol. 97, pp. 391–405, 2009.

[15] G. Li, S. Yang, and Z. Nie, "Direction of arrival estimation in time modulated linear arrays with unidirectional phase center motion," *IEEE Transactions on Antennas and Propagation*, vol. 58, no. 4, pp. 1105–1111, April 2010.

[16] Y. Tong and A. Tennant, "Simultaneous control of sidelobe level and harmonic beam steering in time-modulated linear arrays," *Electronics Letters*, vol. 46, no. 3, pp. 201–202, Feb 2010.

[17] A. Tennant, "Experimental two-element time-modulated direction finding array," *IEEE Transactions on Antennas and Propagation*, vol. 58, no. 3, pp. 986–988, March 2010.

[18] C. He, X. Liang, Z. Li, J. Geng, and R. Jin, "Direction finding by time-modulated array with harmonic characteristic analysis," *IEEE Antennas and Wireless Propagation Letters*, vol. 14, pp. 642–645, 2015.

[19] H. E. Shanks and R. W. Bickmore, "Four-dimensional electromagnetic radiators," *Canadian Journal of Physics*, vol. 37, no. 3, pp. 263–275, 1959.

[20] J. Bregains, J. Fondevila-Gomez, G. Franceschetti, and F. Ares, "Signal radiation and power losses of time-modulated arrays," *IEEE Transactions on Antennas and Propagation*, vol. 56, no. 6, pp. 1799–1804, 2008.

[21] G. Li, S. Yang, Z. Zhao, and Z.-P. Nie, "A study of AM and FM signal reception of time modulated linear antenna arrays," *Progress In Electromagnetics Research Letters*, vol. 7, pp. 171–181, 2009.

[22] Q. Zhu, S. Yang, R. Yao, M. Huang, and Z. Nie, "Unified time- and frequency-domain study on time-modulated arrays," *IEEE Transactions on Antennas and Propagation*, vol. 61, no. 6, pp. 3069–3076, June 2013.

[23] R. Maneiro-Catoira, J. Brégains, J. García-Naya, and L. Castedo, "On the feasibility of time-modulated arrays for digital linear modulations: A theoretical analysis," *IEEE Transactions on Antennas and Propagation*, vol. 62, no. 12, pp. 6114–6122, Dec. 2014.

[24] R. Maneiro-Catoira, J. Brégains, J. A. García-Naya, and L. Castedo, "Time-modulated arrays for digital communications," in *Antennas and Propagation Society International Symposium (APSURSI), 2014 IEEE*, July 2014, pp. 1760–1761.

[25] Q. Zhu, S. Yang, P. Rocca, and Z. Nie, "Signal-to-noise ratio and time-modulated signal spectrum in four-dimensional antenna arrays," *IET Microwaves, Antennas Propagation*, vol. 9, no. 3, pp. 264–270, 2015.

[26] C. He, X. Liang, B. Zhou, J. Geng, and R. Jin, "Space-division multiple access based on time-modulated array," *IEEE Antennas and Wireless Propagation Letters*, vol. 14, pp. 610–613, 2015.

[27] R. Maneiro-Catoira, J. Brégains, J. A. García-Naya, and L. Castedo, "Time-modulated arrays for digital communications in multipath scenarios," in *Proc. of 2015 IEEE Antennas and Propagation Society International Symposium (APSURSI)*, Jul. 2015, p. 10.1109/APS.2015.7304795.

[28] G. Bogdan, M. Jarzynka, and Y. Yashchyshyn, "Experimental study of signal reception by means of time-modulated antenna array," in *Proc. of 2016 21st International Conference on Microwave, Radar and Wireless Communications (MIKON)*, May 2016, pp. 1–4.
[29] Y. Yashchyshyn, K. Derzakowski, P. R. Bajurko, J. Marczewski, and S. Kozłowski, "Time-modulated reconfigurable antenna based on integrated s-pin diodes for mm-wave communication systems," *IEEE Transactions on Antennas and Propagation*, vol. 63, no. 9, pp. 4121–4131, Sept 2015.
[30] A. Goldsmith, *Wireless Communications*. Cambridge University Press, 2005.
[31] P. Rocca, Q. Zhu, E. Bekele, S. Yang, and A. Massa, "4-D arrays as enabling technology for cognitive radio systems," *IEEE Transactions on Antennas and Propagation*, vol. 62, no. 3, pp. 1102–1116, March 2014.
[32] M. A. M.K.Simon, *Digital Communication over Fading Channels*, 2nd ed. Wiley, 2005.
[33] B. Sklar, *Digital Communications*, 2nd ed. Prentice Hall, 2001.
[34] D. Tse and P. Viswanath, *Fundamentals of wireless communication*. Cambridge University Press, 2005.
[35] S. Yang, Y. Gan, and P. Tan, "Evaluation of directivity and gain for time-modulated linear antenna arrays," *Microw. Opt. Technol. Lett.*, vol. 42, p. 167–171, 2004.
[36] M. K. Simon and D. Divsalar, "Some new twists to problems involving the gaussian probability integral," *IEEE Transactions on Communications,*, vol. 46, no. 2, pp. 200–210, Feb 1998.
[37] M. K. Simon and M.-S. Alouini, "A unified approach to the performance analysis of digital communication over generalized fading channels," *Proceedings of the IEEE*, vol. 86, no. 9, pp. 1860–1877, Sep 1998.
[38] "MiniCircuits," http://www.minicircuits.com.

Roberto Maneiro-Catoira received the Telecommunications Engineering degree from the University of Vigo, Spain, in 1995 and the Master of Information and Telecommunications Technologies for Mobile Networks degree in 2012 from the University of A Coruña, Spain, in 2012. He worked from 1996 to 1997 at Egatel company focused on the Research and Development in the field of TV and Radio digital communications. From 1997 to 2000 he was with Siemens Mobile Networks as GSM access network deployment manager. From 2000 to 2003 he worked at Nortel Networks as UMTS network integration manager. From 2003 he is fully dedicated to teaching Siemens Simatic Programmable Logic Devices as well as mathematics for different levels, both for private and public organisms. Actually he is working towards his Ph.D. about dynamic arrays for digital communications in the Electronic Technology and Communications Group (GTEC) at the University of A Coruña.

Julio C. Brégains received in 2000 the B.S. in Electrical Engineering from the National University of the Northeast, Argentina, and the Industrial Engineering degree from the University of León, Spain, in 2006. In 2007 he obtained with honors a Ph.D. degree in Applied Physics from the University of Santiago de Compostela (USC), Spain. He is currently an Assistant Professor of Electronics at the Department of Electronics and Systems of the School of Informatics, at the University of A Coruña, Spain. He is also currently a member of the Electronic Technology and Communications Group (GTEC), at that department. He has co-authored over 80 international journal and conference papers, having received awards for three of them. His research interests include high-frequency electronics, software development for solving electromagnetic problems, antenna array pattern synthesis and design, and variational problems applied to field theory.

José A. García-Naya studied Computer Engineering at the University of A Coruña (UDC), Spain, where he obtained his M.Sc. degree in 2005, and his Ph.D. degree with the distinction "Doctor with European Mention" in 2010. Since 2005 he is with the Group of Electronics Technology and Communications (GTEC) at the UDC, where he is currently Associate Professor. José A. García-Naya is coauthor of more than seventy papers in peer-reviewed international journals and conferences. He has also been member of the research team in more than forty research projects funded by public organizations and private companies. His research interests are in the field of wireless communication systems, with special emphasis on their experimental evaluation.

Luis Castedo was born in Santiago de Compostela, Spain, in 1966. He received the Ingeniero de Telecomunicación and Doctor Ingeniero de Telecomunicación degrees, both from Polytechnic University of Madrid, Spain, in 1990 and 1993, respectively. From November 1994 to October 2001, he was an Associate professor in the Department of Electronics and Systems at University of A Coruña, Spain, where he is currently Full Professor. He has been chairman of the Department between 2003 and 2009. Luis Castedo is coauthor of more than one hundred papers in peer-reviewed international journals and conferences. He has also been principal researcher in more than thirty research projects funded by public organizations and private companies. His research interests are signal processing and digital communications with special emphasis on blind adaptive filtering, estimation/equalization of MIMO channels, space-time coding and prototyping of digital communication equipments.

Paolo Rocca received the MS degree in Telecommunications Engineering from the University of Trento in 2005 (summa cum laude) and the PhD Degree in Information and Communication Technologies from the same University in 2008. He is currently Associate Professor at the Department of Information Engineering and Computer Science (University of Trento) and a member of the ELEDIA Research Center. Dr. Rocca is the author/co-author of over 250 peer reviewed papers on international journals and conferences.

Dr. Rocca has been a visiting Ph.D. student at the Pennsylvania State University (U.S.A.), at the University Mediterranea of Reggio Calabria (Italy), and a visiting researcher at the Laboratoire des Signaux et Systèmes (L2S Supèlec, France) in 2012 and 2013. Moreover, he has been an Invited Associate Professor at the University of Paris Sud (France) in 2015. Dr. Rocca has been awarded from the IEEE Geoscience and Remote Sensing Society and the Italy Section with the best PhD thesis award IEEE-GRS Central Italy Chapter. His main interests are in the framework of antenna array synthesis and design, electromagnetic inverse scattering, and optimization techniques for electromagnetics. He serves as an Associate Editor of the IEEE Antennas and Wireless Propagation Letters.

Lorenzo Poli received the M.S. degrees in Telecommunication Engineering from the University of Trento, Italy, in 2008, and the PhD degree from the International Doctoral School in Information and Communication Technology in 2012. He is a member of the ELEDIA Research Center. His research activities are focused on the solution of antenna array synthesis and electromagnetic inverse scattering problems.